Nitric/Nitrous Acid Equilibria in Supercritical Water

Jerzy Chlistunoff,[†] Kirk J. Ziegler,[†] Leon Lasdon,[‡] and Keith P. Johnston*[,†]

Department of Chemical Engineering and Department of Management Science and Information Systems, The University of Texas at Austin, Austin, Texas 78712

Received: September 16, 1998; In Final Form: January 13, 1999

UV−vis spectroscopy was utilized to measure the decomposition of aqueous HNO_3 solutions above 300 °C, in some cases with added NaOH, H_2O_2, and/or $NaNO_2$, to form NO_2, HNO_2, NO, N_2O, and oxygen. Individual bands corresponding to HNO_2 and NO_2 were deconvoluted from the spectra up to 400 °C. With constrained nonlinear optimization, areas of these bands were used to determine extinction coefficients of NO_2 and HNO_2 and equilibrium constants for the reactions: $HNO_3 \rightleftharpoons H^+ + NO_3^-$; $2HNO_3 \rightleftharpoons H_2O + 2NO_2 + (1/2)O_2$; $2NO_2 + H_2O \rightleftharpoons HNO_3 + HNO_2$; $2HNO_2 \rightleftharpoons H_2O + 2NO + (1/2)O_2$; $2NO \rightleftharpoons N_2O + (1/2)O_2$; $(Na^+)(NO_3^-) \rightleftharpoons Na^+ + NO_3^-$.

Introduction

Reactions involving NO, NO_2, H_2O, HNO_3, HNO_2, and O_2 in the gas phase play a crucial role in nitric acid production, combustion,[1] and waste incineration. These reactions have been studied extensively in both the gas phase and for a gas phase in contact with an aqueous phase, typically at temperatures below 100 °C.[2−5] The amount of NO_x in exhaust gases may be lowered by catalytic reduction with NH_3 to form N_2, or conversely, NO_x may be used to oxidize ammonia wastes to N_2.[6−8]

More recently, NO_x chemistry has been studied in hydrothermal oxidation (HO) (also called supercritical water oxidation (SCWO)).[9,10] In HO, an aqueous waste containing organics is oxidized by oxygen in supercritical water (SCW), i.e., at temperatures higher than 374 °C (typically around 500 °C and above 220 bar). Thermodynamics and kinetics favor significantly less NO_x at the relatively low temperatures in HO compared with incineration where temperatures are typically 1200 °C or more.[11] Kinetic studies of oxidation reactions of organic compounds by nitrates suggested that the reactive species in SCW solutions of nitrates can be NO_2.[12] Recently, it was suggested that nitrates present in certain high level and mixed nuclear wastes could be used as an oxidizing agent instead of oxygen in the HO pretreatment of these wastes.[13−15] It has been proposed that ammonium nitrate recovered from demilitarized rocket motors may be utilized as an oxidizing agent in HO.[16] NO_x chemistry is also important in rapid hydrolysis of metal nitrates to form submicrometer metal oxide crystals.[17,18]

Fundamental studies of nitrogen chemistry in SCW are relatively rare due to corrosion and the challenges from high pressures and temperatures. Brill and co-workers studied kinetics and mechanisms for decomposition reactions of a variety of nitrogen-containing compounds in SCW including thermal decomposition of hydroxylammonium nitrate,[19] urea and guanidinium nitrate,[20] and ethylenediammonium dinitrate[21] by using FTIR and Raman spectroscopy. Spohn and Brill[22] studied ion pair formation in concentrated aqueous solutions of zinc, cadmium, lithium, and sodium nitrates up to 450 °C by Raman spectroscopy, which is very sensitive to contact interactions. The dissociation of nitric acid under hydrothermal conditions up to 250 °C was studied by Raman spectroscopy[23] and up to 319 °C from the heat of dilution of concentrated HNO_3 solutions.[24] Marshall and Slusher obtained HNO_3 dissociation constants indirectly from solubilities of magnesium sulfate[25] (up to 370 °C) and calcium sulfate[26] (up to 350 °C). However, Marshall and co-workers[26−28] found that nitric acid decomposes reversibly to nitrogen oxides and water at elevated temperatures even below the critical point of water.[23,25,26]

Chemical reaction equilibria may be measured quantitatively in hydrothermal solution by UV−vis spectroscopy. As demonstrated by Seward and co-workers,[29−31] complex equilibria in hydrothermal solutions can be elucidated by spectral deconvolution techniques[29] and nonlinear regression procedures.[29,31] Chemical equilibria involving H_2CrO_4 and $HCrO_4^-$ were measured quantitatively up to 420 °C.[32] A series of relatively stable organic pH indicators has been developed to measure pH and monitor acid−base equilibria up to 420 °C.[33−37] These studies demonstrate that UV−vis spectroscopy is well suited for obtaining quantitative equilibrium constants in SCW.

The objective of this work was to characterize and quantify chemical reaction equilibria involving nitric acid and its decomposition products with UV−vis spectroscopy in SCW. Because of the possibility for severe corrosion, a new apparatus was developed in which the solutions contacted only titanium, gold, and sapphire and could be flushed rapidly. The Results and Discussion begins with a description of changes in spectra resulting from adding NaOH, H_2O_2, $NaNO_2$, or mixtures of these compounds to HNO_3 solutions. Here, the goal is to determine qualitatively which decomposition products are present based on these changes in spectra. Next, spectral deconvolution and peak assignment are discussed. From the areas of the deconvoluted spectra, a large-scale generalized reduced gradient (LSGRG2) optimization model[38] was utilized to determine optimal values of the extinction coefficients and equilibrium constants in conjunction with the concentrations of the decomposition products. The density effect on equilibrium constants is discussed as a function of changes in polarity upon reaction. The equilibrium constants are also utilized to calculate speciation

* To whom correspondence should be addressed.
[†] Department of Chemical Engineering.
[‡] Department of Management Science and Information Systems.

10.1021/jp983745o CCC: $18.00
Published on Web 03/02/1999

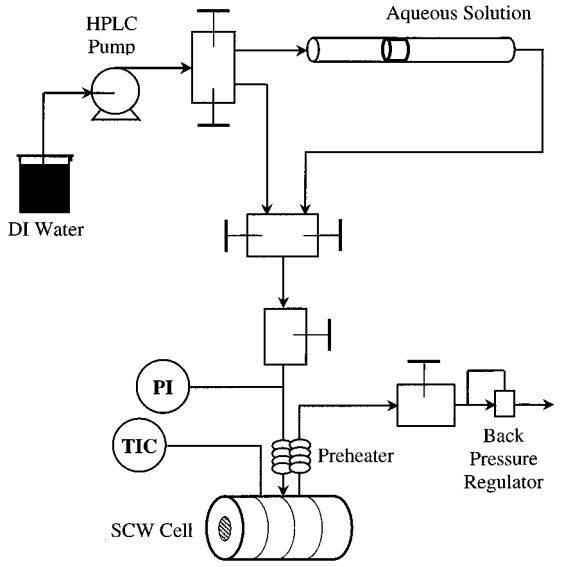

Figure 1. Stopped flow apparatus for UV−vis spectroscopy of corrosive solutions in SCW.

diagrams. Quantitative knowledge of chemical reaction equilibria of nitrogen chemistry is highly relevant to understanding hydrolysis and oxidation reactions, corrosion, materials science, and separation processes in hydrothermal solution.

Experimental Section

The experimental apparatus was similar to one applied previously.[32,39] Spectra were obtained in a titanium optical cell equipped with two sapphire windows with an aperture of 5 mm and a path length of 1 cm. A modification was made to avoid pumping highly corrosive HNO_3 solutions through the HPLC pump (Figure 1). The solutions were added to the top of a 11/16″ i.d. × 1″ o.d. 6 foot long stainless steel tube equipped with a stainless steel piston and polypropylene o-ring seals. Pure deionized water was pumped with an HPLC pump into the tube below the piston to displace the solution through a titanium preheater (0.03″ i.d., 2 foot length) into the titanium optical cell. A bypass line was used to flush the cell with pure water. The typical time required to exchange the solution in the cell was around 3 min. After the cell was flushed with water or a fresh solution, the spectra were recorded. The spectrum for pure water (baseline) was measured immediately after the temperature attained its steady preset value. The spectra for the solutions were measured after additional flushing of the cell with 1 mL of the solution and reequilibrating the temperature. Typically four spectra were recorded at different pressures without flushing the cell between experiments. The solution residence time, which did not exceed 6 min, was usually sufficiently short to produce only minor corrosion as well as negligible changes in the spectra.

Carbon dioxide free, approximately 0.5 M stock NaOH (analytical grade, EM Science) solution was prepared and standardized using generally accepted procedures.[40] A stock solution (approximately 0.5 M) of HNO_3 (70%, AR, Mallinckrodt) was standardized by titration with the above NaOH standard solution. Approximately 0.25 M $NaNO_2$ solution was obtained by dissolving a sample of analytical grade $NaNO_2$ (EM Science) in a known volume of deionized water. Its concentration was determined by a classical Lunge method,[41] i.e., by titration with a known volume of a standard $KMnO_4$ solution. This method is accurate to within 0.5−1%. The NaOH and $NaNO_2$ stock solutions were prepared frequently, to reduce errors associated with absorption of CO_2 or decomposition

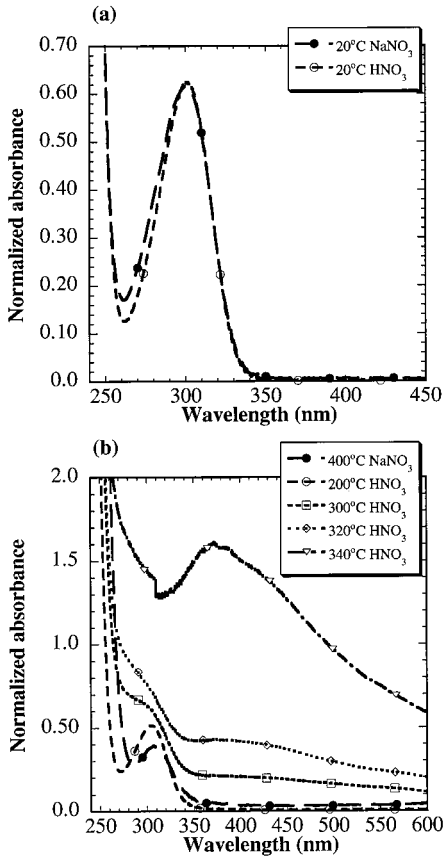

Figure 2. Spectra of 0.0928 mol kg^{-1} HNO_3 (filled symbols) and $NaNO_3$ (open symbols), pressure 34.5 MPa.

($NaNO_2$). Hydrogen peroxide (30%, EM Science) concentration was determined before each experiment by titration with a standard $KMnO_4$ solution.[41]

With a few exceptions, the feed solutions were thoroughly deoxygenated by purging with nitrogen. The solutions containing H_2O_2 as well as mixtures of HNO_3 and $NaNO_2$ solutions were not deoxygenated, because of H_2O_2 decomposition upon shaking and evolution of NO, respectively. In these cases, however, the solutions were prepared immediately before each experiment in freshly deoxygenated water. After brief but thorough mixing, the solution was placed in the stainless steel tube and immediately isolated and pressurized. The estimated concentration of oxygen in these feed solutions was around 4×10^{-5} mol kg^{-1} based on the partial pressure of oxygen in air and the solubility of O_2 in water. Other details of the experimental procedures can be found elsewhere.[32]

Results and Discussion

Concentrated $NaNO_3$ and HNO_3 Solutions from 20 to 400 °C. The spectrum of nitrate ion in water is characterized by two principal bands, as shown in Figure 2. The short-wavelength band ($\lambda = 200.3$ nm at ambient conditions) is very strong ($\epsilon = 9600$). While the high ϵ of this band is beneficial, its λ is not, since a variety of other species also absorb strongly here, including other NO_x species, OH^- via charge transfer to solvent, and the sapphire windows. The long-wavelength band, centered at around 300 nm, is very weak with an extinction coefficient on the order of 7, which is too small to be of use.

The effect of temperature on the spectra of 0.0928 mol kg^{-1} HNO_3 and 0.0928 mol kg^{-1} $NaNO_3$ solutions is shown in Figure 2. Within limits of experimental error, the spectra of these solutions at room temperature are identical (Figure 2a), in

TABLE 1: Compositions of the Classes of Solutions Studied.

class	HNO_3 mmol kg^{-1}	NaOH mmol kg^{-1}	H_2O_2 mol kg^{-1}	$NaNO_2$ mmol kg^{-1}
I	7.736−38.68	0.0	0.0	0.0
II	19.34	1.237−12.37	0.0	0.0
III	23.20	0.0	0.182−0.931	0.0
IV[a]	0.0−16.28	0.0	0.0	4.52−20.8
V	15.40	7.667	0.0	5.42
	13.73	4.617	0.0	7.03

[a] Total nitrogen concentration was 0.0208 mol kg^{-1}.

accordance with the fact that nitric acid is completely dissociated. However, an increase in temperature at a constant pressure of 34.5 MPa leads to changes in HNO_3 (open symbols) and $NaNO_3$ (filled symbols). While changes in $NaNO_3$ spectra up to 400 °C can be regarded as minor (Figure 2b), temperature exerts a significant effect on the HNO_3 spectra. A temperature increase from 20 to 200 °C leads to increased overlap of the 300 and 200 nm bands. Since nitric acid becomes a weaker acid at elevated temperatures, these changes may reflect formation of molecular HNO_3.

At temperatures equal to or higher than 300 °C, an additional broad band centered around 370 nm, appears. This band grows significantly with temperature. While part of this increase is reversible and the nitrate band at 300 nm can be restored after cooling the cell, the measured absorbance does not drop back to zero at wavelengths longer than those corresponding to the nitrate band. The reversible changes at temperatures greater than or equal to 300 °C represent reversible decomposition of nitric acid, as previously suggested by Marshall and co-workers, based upon visual observation of HNO_3 samples in silica capillary tubes.[27] The residual absorption is still observed even after the cell is flushed with pure deionized water, due to the presence of a uniform brown deposit on the windows. The amount of the deposit increases with the nitric acid residence time in the cell. The brown deposit is believed to be titanium dioxide, which is formed when the hot solution containing Ti corrosion products contacts the cooler windows. Indeed, extensive use of the cell with these concentrated HNO_3 solutions resulted in formation of pits on the flat Ti surfaces remaining in contact with the gold seals. The corrosion led to serious leaks and irreproducible results due to inaccurate correction of the spectra for the baseline.

The corrosion of the cell and deposition of TiO_2 on the windows was curtailed by lowering the acid concentration to a level of $2-3 \times 10^{-2}$ mol kg^{-1}, which is also more suitable for equilibrium constant determinations. However, the changes occurring to the weak 300 nm band could no longer be accurately measured in our 1 cm cell. Fortunately, the light absorption by the HNO_3 decomposition products in the dilute HNO_3 solutions was sufficiently high to be measured quantitatively at temperatures exceeding 360 °C. Preliminary experiments revealed, however, that the spectra measured at 360 °C were not reproducible, because of either a relatively slow approach to equilibria or TiO_2 deposition. At 420 °C, on the other hand, leaks constituted a serious problem. At temperatures of 380 and 400 °C, equilibrium was achieved rapidly and leaks were minor, such that quantitative experiments could be performed.

Spectra of Nitric Acid and Its Mixtures with Sodium Hydroxide, Hydrogen Peroxide, and Sodium Nitrite at 380 and 400 °C. The experiments were grouped in five distinct classes depending on the feed solution composition (Table 1). The various classes were designed to manipulate the relative equilibrium concentrations of the nitrogen species, especially the oxidation states, to be able to obtain equilibrium constants from the spectra. The first class consisted of pure nitric acid solutions (class I). In class II, these solutions were partially neutralized solutions with NaOH to form NO_3^-, which was shown above to be much more stable than HNO_3. Class III included H_2O_2 as an oxidant. Mixtures of $HNO_3 + NaNO_2$ were used in class IV to shift the oxidation states, while NaOH was added to this mixture in class V.

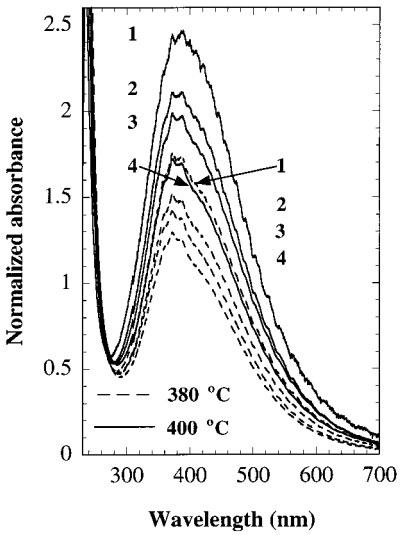

Figure 3. Spectra of 3.868×10^{-2} mol kg^{-1} HNO_3 solutions at two temperatures and four pressures. Pressure (MPa): 27.6 (1); 31.0 (2); 34.5 (3); 41.3 (4). The spectra are corrected for density of water. Note similarity of spectrum 1 at 380 °C and spectrum 4 at 400 °C, which were obtained at similar densities, i.e., 0.506 and 0.533 g cm^{-3}, respectively.

Typical spectra for a class I experiment are shown in Figure 3. In this class, spectra were time independent for times not exceeding 20 min. The spectra were reversible with changes in temperature and pressure, suggesting that decomposition products revert back to the starting material. The large asymmetric band at 385 nm decreases with an increase in density, especially at low densities. The band position, shape, and fine structure are all very similar to that observed for NO_2 spectra in the gas phase.[42−45] However, these spectra do not correspond to NO_2 only. A distinct set of small peaks, whose relative contribution to the measured absorbance changes with temperature and pressure, can be seen on top of the large NO_2 band. The relative contribution from the set of small peaks decreases with increasing concentration (absorbance) of NO_2 resulting from decreasing solution density. A similar but somewhat weaker effect was also seen at a constant temperature and pressure when the NO_2 concentration increased due to an increase in the HNO_3 feed concentration. The fact that the relative contribution of the small peaks increases when the NO_2 concentration decreases suggests that these small peaks are not due to the presence of N_2O_4, i.e., NO_2 dimer. The dimerization reaction occurs to a limited extent at room temperature[3,42,46,47] in the gaseous phase, and the degree of dimerization decreases strongly with increasing temperature.[46,47] Thus, dimerization is extremely unlikely at the high temperatures employed in this study. In addition, N_2O_4 absorbs light at shorter wavelengths, and the absorption band does not exhibit any fine structure.[42]

The general behavior observed for partially neutralized HNO_3 solutions (class II, Table 1) was very similar to that exhibited by pure nitric acid solutions. Solutions with equal feed concentrations of H^+ at ambient temperature, i.e., pure nitric acid solutions of concentration m^o and partially neutralized

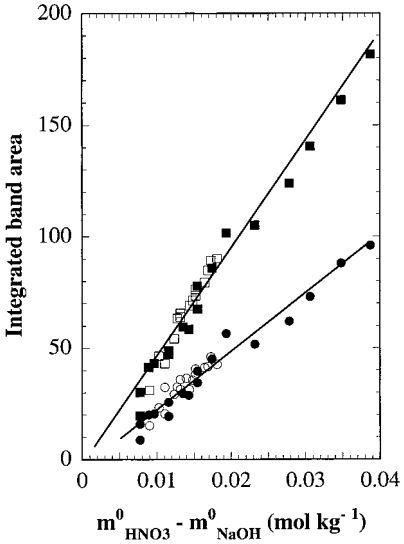

Figure 4. The NO_2 band area integrated over 450−600 nm (bottom line) and 330−450 nm (top line) plotted against the concentration of nitric acid in pure nitric acid solutions (filled symbols) or excess of nitric acid in nitric acid/NaOH mixtures (open symbols): temperature 380 °C, pressure 27.6 MPa.

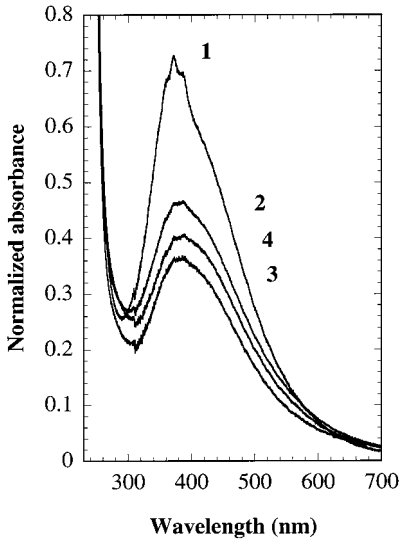

Figure 5. Spectra of 2.320×10^{-2} mol kg^{-1} HNO_3 with addition of hydrogen peroxide: temperature 380 °C, pressure 41.3 MPa. Hydrogen peroxide concentration (mol kg^{-1}): 0.0 (1); 0.262 (2); 0.546 (3); 0.906 (4).

HNO_3 solutions with an excess acid concentration equal to m^o, had almost identical spectra in supercritical water. This result is shown in Figure 4, where the integrated band areas in two wavelength ranges are plotted versus feed excess H^+ concentration. The band area, integrated over the wavelength range 450−600 nm, is believed to correspond to a single species (NO_2), because the ratios of absorbances measured at a given temperature and pressure for any two solutions were essentially independent of the wavelength in this range. In contrast, the area integrated over the wavelength range 330−450 nm includes the contribution from the substance(s) giving rise to the set of small peaks. As seen in Figure 4 and the associated spectra, this contribution, even though relatively small, is similar for pure nitric acid solutions and partially neutralized HNO_3 solutions with equal excess H^+ feed concentration.

Addition of an excess oxidant such as H_2O_2, which decomposes to oxygen and water,[48,49] to a 0.0232 mol kg^{-1} HNO_3 solution removes the set of small peaks centered around 370 nm as shown in curves 3 and 4 of Figure 5 (class III, Table 1). The large NO_2 band is not affected significantly by H_2O_2. At 380 °C and all the pressures studied, the NO_2 band initially decreases and then increases slightly as the oxygen content increases. At 400 °C, the NO_2 band decreases monotonically as the feed H_2O_2 concentration increases from 0.18 to 0.93 mol kg^{-1}.

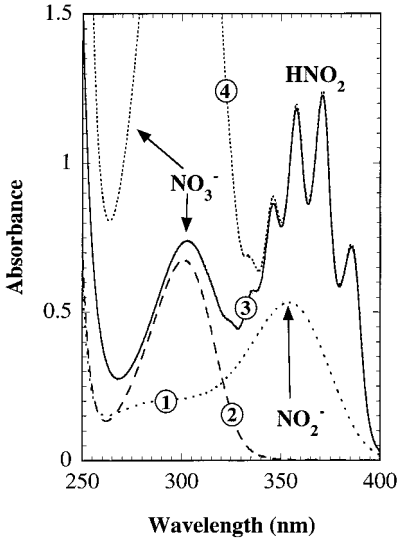

Figure 6. Room-temperature spectra of nitrates, nitrites, and the corresponding acids and assignment of the bands: (1) 2.26×10^{-2} mol dm^{-3} $NaNO_2$; (2) 9.280×10^{-2} mol dm^{-3} $NaNO_3$; (3) 2.26×10^{-2} mol dm^{-3} $NaNO_2$ + 9.280×10^{-2} mol dm^{-3} HNO_3; (4) 2.26×10^{-2} mol dm^{-3} $NaNO_2$ + 0.4176 mol dm^{-3} HNO_3.

The stability of NO_2 versus the instability of the species represented by the set of small peaks in the presence of oxygen (curve 1 and 2 in Figure 5) suggests that the yet unidentified species contains nitrogen in an oxidation state lower than +4. Among known H_yNO_x (x, $y \geq 0$) species, only NO_2^- and unstable HNO_2 (disproportionates to HNO_3 and NO) absorb light in this range.[50−54] Their spectra were measured at ambient conditions (Figure 6) and agreed well with literature data.[50−54] The positions, intensities, and shapes of the spectra shown in Figure 6 strongly suggest that the set of small bands on top of the NO_2 band in hydrothermal HNO_3 solutions corresponds to the HNO_2/NO_2^- couple.

The differences in the influence of oxygen on the HNO_2/NO_2^- and NO_2 bands can be explained qualitatively in a simple manner in terms of the following equilibrium:

$$2NO_2 + H_2O \rightleftharpoons 2HNO_2 + (1/2)O_2 \qquad (1)$$

Addition of oxygen shifts this equilibrium to the left and therefore explains the relative decrease of the HNO_2/NO_2^- content versus that of NO_2 in Figure 5. One should note, however, that this explanation does not include HNO_3 as well as any nitrogen species with an oxidation state lower than +3, such as NO, which, as suggested by literature data,[55] can also be present in our case. A more quantitative explanation, which includes these species, is given in the speciation diagrams below.

Figure 7 shows the effect of nitrite on the spectra of HNO_3 for a fixed total nitrogen concentration of 0.0208 mol kg^{-1} (class IV). An increase in the $NaNO_2$ concentration leads to a significant decrease in the NO_2 band. At the same time, the set of small bands at 370 nm does not seem to be affected strongly for a molar ratio of $NaNO_2$ to HNO_3 up to 1:1. At higher $NaNO_2$ to HNO_3 ratios, the set of small bands (HNO_2/NO_2^-) is gradually replaced by a single band (NO_2^-) at a wavelength similar to

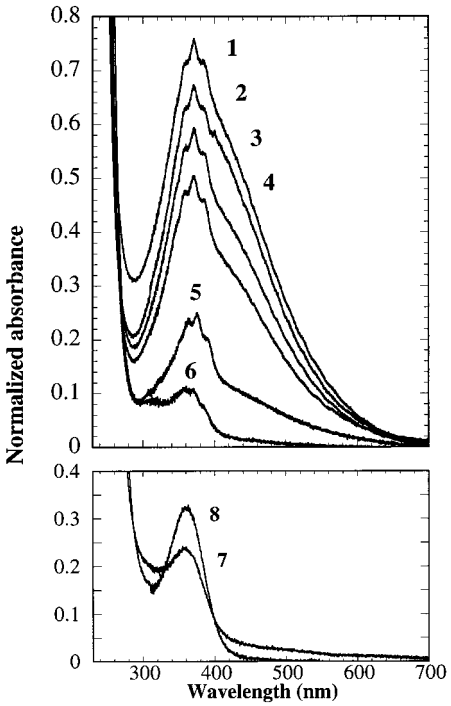

Figure 7. Spectra of $HNO_3/NaNO_2$ mixtures with a total nitrogen content of 0.0208 mol kg^{-1}: temperature 380 °C, pressure 31.0 MPa. $NaNO_2$ mole fraction: 0.218 (1); 0.260 (2); 0.385 (3); 0.442 (4); 0.549 (5); 0.635 (6); 0.778 (7); 1.0 (8).

that measured in pure $NaNO_2$ solution (curve 8). As could be expected for a salt of a relatively weak acid, sodium nitrite solution was found to be a rather strong base in supercritical water, as manifested by significant corrosion of the sapphire windows.[32]

The observed changes in the spectra resulting from addition of $NaNO_2$ to nitric acid (Figure 7) further support our assignment of the bands. Because the total nitrogen content is fixed, the amount of HNO_3 in the feed mixture decreases. Consequently products from the decomposition of HNO_3, i.e., NO_2 and HNO_2/NO_2^- decrease. However, the total nitrite concentration (small bands) does not decrease since the loss in HNO_2/NO_2^- is compensated for by the greater amount of nitrite introduced in the feed. Alternatively, the same effects may be explained in terms of the net oxidation state of nitrogen in the mixture. The decrease in the net oxidation state of nitrogen in the feed mixture leads to the relative increase of the lower oxidation state (HNO_2/NO_2^-) versus that of the higher oxidation state (NO_2).

For mixtures with a high $NaNO_2$ to HNO_3 ratio (spectra 6 and 7 in Figure 7), the concentration of NO_2 is negligible. The composite HNO_2/NO_2^- band is also much smaller than expected for pure NO_2^- or HNO_2 solutions with identical total nitrogen content. While part of the nitrogen in these solutions can be in the form of NO_3^-, which has a weak absorption band around 300 nm (see Figure 6 and Figure 7 curve 6), other nitrogen species may also be present such as NO or N_2O which absorb below 280 nm.[56]

Experiments for mixtures of nitric acid, sodium hydroxide, and sodium nitrite (class V) were performed to further increase the ratio of HNO_2/NO_2^- to NO_2 over the values in class IV. As shown by the reaction

$$2H^+ + 2NO_3^- \rightleftharpoons 2NO_2 + H_2O + (1/2)O_2 \qquad (2)$$

the addition of a base (NaOH) may be expected to lower the NO_2, as was observed (not shown).

Deconvolution of the Spectra. As shown in the preceding section, the only distinct bands in the measured spectra are those corresponding to NO_2 and HNO_2/NO_2^-. Among other species which can absorb light in the visible and near-UV ranges are HNO_3, NO_3^-, N_2O_4, and N_2O_3. The steep increases in absorbance at wavelengths shorter than 280 nm cannot be used for analytical purposes, since so many nitrogen species absorb in this range. Above, we have already eliminated the possibility of N_2O_4.

The HNO_3 and NO_3^- low-energy bands are very weak[57] (Figures 2 and 6). The absorbance of a 0.02 mol kg^{-1} HNO_3 solution at 300 nm resulting from the presence of HNO_3 or NO_3^- would not exceed 0.14 if there was no decomposition and assuming temperature-independent extinction coefficients. Because a significant amount of HNO_3 decomposes, the remaining absorbance is too low to be determined accurately, especially after including effects due to the overlap with higher energy bands (Figure 2), absorbance from decomposition products, and light scattering by the TiO_2 deposit on the windows. Consequently, we decided to exclude NO_3^- and HNO_3 bands from spectral deconvolution.

N_2O_3 has a weak band ($\epsilon \approx 20$) centered around 620 nm[58] and absorbs strongly in the UV region. The estimated extinction coefficient of N_2O_3 at 280 nm is 290.[59] Since the measured absorbance at 280 nm did not exceed 0.4 in a 2×10^{-2} mol kg^{-1} HNO_3 solution, the maximum possible N_2O_3 concentration could not exceed 1.4×10^{-3} mol kg^{-1} resulting in a normalized absorbance of 0.03 at 620 nm. Similar calculations for $HNO_3/NaNO_2$ mixtures reveal that the absorbance due to N_2O_3 at 620 nm is also insignificant. In addition, gas-phase data suggest that N_2O_3 should dissociate almost completely to NO and NO_2 at our temperatures.[6,47,60,61] As was the case for nitrate, we think that the N_2O_3 band at 620 nm, if present, is too small to be accurately measured and deconvoluted from the spectra.

Another species that was considered was the solvent separated ion pair $(H^+)(NO_2^-)$ or, in solutions containing Na^+, $(Na^+)(NO_2^-)$. These species will now be shown to be much less stable than HNO_2. The dissociation constant of nitrous acid under our experimental conditions can be roughly estimated to be on the order of 10^{-8} or less at 380 °C and solution densities in the range 0.5−0.6 g cm^{-3} based on low-temperature data[62−64] and comparison with other acids of comparable strength in supercritical water.[65,66] Dissociation constants for 1:1 alkali metal salts at densities from 0.5 to 0.6 g cm^{-3} are typically between 10^{-1} and 10^{-2} at 380 °C.[66,67] Based on these equilibrium constants, comparable concentrations of HNO_2 and $(Na^+)(NO_2^-)$ would exist for H^+ to Na^+ equilibrium concentration ratios lower than 10^{-6}, i.e., H^+ concentration on the order of 10^{-8} mol kg^{-1}, which is unlikely in acidic media. For similar reasons, the concentration of $(H^+)(NO_2^-)$ may be expected to be insignificant. Therefore, we chose to exclude $(H^+)(NO_2^-)$ and $(Na^+)(NO_2^-)$ bands from the spectral deconvolution.

Our final procedure was to deconvolute the spectra with only five Gaussian peaks, four of them representing HNO_2 and one representing NO_2. Fixed widths and positions were used for the HNO_2 bands as determined from the spectra where HNO_2 bands were the strongest (see above). A wavenumber range of 3×10^4 to 5×10^4 cm^{-1} (333−500 nm) was used to achieve an accurate fit for the asymmetric NO_2 peak. The position and width of this peak was allowed to vary. Extensive calculations revealed that the NO_2 peak position peak width varied randomly (Table 2), most likely because of the large peak width and the imperfect baseline correction. Spectra obtained from class IV experiments with a $NaNO_2$ to HNO_3 ratio higher than ap-

TABLE 2: Deconvolution of the Spectra with Five Gaussian Peaks at 380−400 °C and 27.6−41.3 MPa[a]

band	species	λ nm	$1/\lambda$ cm^{-1}	peak width cm^{-1}	peak area ratio[b] class I	class II[c]	class III[d]	class IV
1	NO_2	385 ± 7		1134 ± 48				
2	HNO_2	386.1	25900	50	1	1	1	1
3	HNO_2	371.7	26900	90	0.33 ± 0.04	0.32 ± 0.07	0.25 ± 0.09	0.34 ± 0.03
4	HNO_2	358.4	27900	70	0.64 ± 0.10	0.65 ± 0.16	0.99 ± 1.00	0.70 ± 0.11
5	HNO_2	348.4	28700	130	0.58 ± 0.20	0.69 ± 0.23	2.31 ± 7.21	0.69 ± 0.14

[a] The errors listed are mean standard deviations. [b] Peak area relative to band 2. [c] After removing four data points which deviated strongly from the mean. [d] Significant scatter in these data result from the extremely small nitrous acid bands in the presence of oxygen.

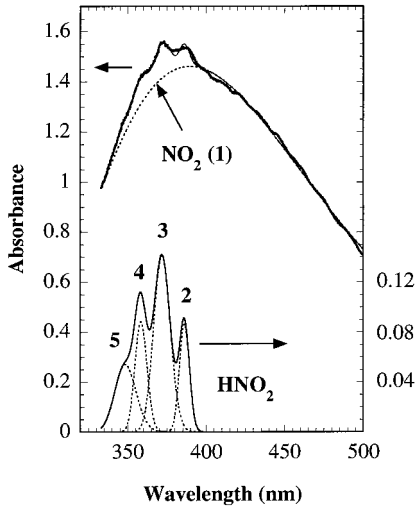

Figure 8. Peak fitting results for a 0.03480 mol kg^{-1} HNO_3 solution at 27.6 MPa and 380 °C. The individual bands obtained from the fitting are drawn with dotted lines. Thick and thin full lines in the upper portion of the graph represent the measured and fitted spectra, respectively.

proximately 1:1 (curves 6−8 in Figure 7) were excluded, since these solutions obviously contained nitrites whose bands interfered with these of HNO_2. The parameters for the HNO_2 bands were averages of the values obtained from deconvoluting individual spectra; typical results of deconvolution are quite accurate as shown in Figure 8. As shown in Table 2, the ratio of each band to band 2 was relatively constant, indicating only one species produced the fine structure and that the fits were quite accurate. An exception is H_2O_2 class III experiments where nitrous acid peaks were extremely small (Figure 5) and the errors were correspondingly large (Table 2).

The rest of this section describes other deconvolution techniques that were unsuccessful and not adopted. Because the NO_2 band was extremely broad, it was attempted to fit the band with two Gaussian bands. However, the changes in the positions and widths of these bands were unacceptably large. As indicated by the spectra measured for $NaNO_2/HNO_3$ mixtures (see Figure 7), the content of NO_2^- in some of these solutions could potentially be significant. Therefore, it was also attempted to fit the spectra with six Gaussian peaks representing a single NO_2 band, the four strongest HNO_2 bands, and a single NO_2^- band (see Figure 6). However, consistent peak positions and widths were obtained only for the four peaks representing HNO_2 in spectra where the HNO_2 bands were the strongest. Because the single NO_2^- band was not different enough from the NO_2 band, it was not possible to deconvolute reliable values of NO_2^- over a wide pH range. Therefore, spectra were not deconvoluted in this study in solutions where the $NaNO_2$ to HNO_3 ratio in the feed was greater than 1.22:1.

Determination of the Equilibrium Constants. Among possible decomposition products of nitric acid, only NO_2 and HNO_2 could be observed in our spectra. Their concentrations, however, could not be determined directly, since their extinction coefficients are unknown under hydrothermal conditions. The NO_2 extinction coefficients in the gas phase have been determined accurately[43−45,68−71] and are strongly dependent upon temperature.[45,70] The NO_2 band fine structure is significantly reduced in SCW, especially at higher densities (see above). Data are unavailable for nitrous acid extinction coefficients versus temperature, most likely due to the low stability of the acid at low temperatures. However, since measured absorbances are unique functions of extinction coefficients and all the equilibria in the system, both the extinction coefficients and the equilibrium constants may be optimized numerically to the experimental data.[29,30] While details of the numerical method are described elsewhere,[72] the basic method and assumptions are presented here.

The equilibrium between most probable species may be represented by the following basic set of reactions:

$$HNO_3 \rightleftharpoons H^+ + NO_3^- \quad (3)$$

$$2HNO_3 \rightleftharpoons H_2O + 2NO_2 + (1/2)O_2 \quad (4)$$

$$2NO_2 + H_2O \rightleftharpoons HNO_3 + HNO_2 \quad (5)$$

$$2HNO_2 \rightleftharpoons H_2O + 2NO + (1/2)O_2 \quad (6)$$

$$2NO = N_2O + (1/2)O_2 \quad (7)$$

$$H_2O \rightleftharpoons OH^- + H^+ \quad (8)$$

$$NaOH \rightleftharpoons Na^+ + OH^- \quad (9)$$

$$(Na^+)(NO_3^-) \rightleftharpoons Na^+ + NO_3^- \quad (10)$$

Less important reactions are

$$(Na^+)(NO_2^-) \rightleftharpoons Na^+ + NO_2^- \quad (11)$$

$$2NO_2 \rightleftharpoons N_2O_4 \quad (12)$$

$$HNO_2 \rightleftharpoons H^+ + NO_2^- \quad (13)$$

$$2HNO_2 \rightleftharpoons N_2O_3 + H_2O \quad (14)$$

$$N_2O_3 \rightleftharpoons NO + NO_2 \quad (15)$$

For reasons specified immediately below, these equilibria (eqs 11−15) were not considered in our model. As explained above, reactions 11 and 12 do not occur to a significant extent under our experimental conditions. As a result of the low dissociation constant of nitrous acid, reaction 13 is shifted far to the left in all the acidic solutions. At ambient conditions, reaction 14 occurs to a significant extent in strongly acidic dehydrating media[52,53,73] but it is not likely to generate significant quantities of N_2O_3

under our experimental conditions because of reaction 15 as discussed above. The following set of equations defined the equilibrium constants in our model:

$$K_a m_{HNO_3} - m_{H^+} m_{NO_3^-} \gamma_\pm^{\,2} = 0 \quad (16)$$

$$K_4 m_{HNO_3}^{\,2} - m_{NO_2}^{\,2} m_{O_2}^{\,1/2} = 0 \quad (17)$$

$$K_5 m_{NO_2}^{\,2} - m_{HNO_3} m_{HNO_2} = 0 \quad (18)$$

$$K_6 m_{HNO_2}^{\,2} - m_{NO}^{\,2} m_{O_2}^{\,1/2} = 0 \quad (19)$$

$$K_7 m_{NO}^{\,2} - m_{N_2O} m_{O_2}^{\,1/2} = 0 \quad (20)$$

$$K_w - m_{H^+} m_{OH^-} \gamma_\pm^{\,2} = 0 \quad (21)$$

$$K_b m_{NaOH} - m_{Na^+} m_{OH^-} \gamma_\pm^{\,2} = 0 \quad (22)$$

$$K_{d,ip} m_{NaNO_3} - m_{Na^+} m_{NO_3^-} \gamma_\pm^{\,2} = 0 \quad (23)$$

where K_a is the dissociation constant of nitric acid, K_w is the ion product of water,[74] K_b is the inverse of the sodium hydroxide association constant as determined by Ho and Palmer,[75] and $K_{d,ip}$ is the $(Na^+)(NO_3^-)$ ion pair dissociation constant. The subscripts defining the remaining equilibrium constants refer to the reaction numbers in the equations above. It was assumed that the individual ionic activity coefficients are not sensitive to specific properties of ions and can be approximated by the mean ionic activity coefficient, $\gamma_\pm$, given by Pitzer:[76]

$$\ln \gamma_\pm = -A_\varphi \left[\frac{\sqrt{I}}{1 + 1.2\sqrt{I}} + \frac{2}{1.2} \ln(1 + 1.2\sqrt{I}) \right] \quad (24)$$

where A_φ is the Debye−Huckel parameter[76] and I is the ionic strength given by

$$I = \frac{1}{2} \sum_i m_i z_i^{\,2} \quad (25)$$

where m_i and z_i are the molalities and charges of all the ionic species in solution.

The model also included, a charge balance,

$$m_{Na^+} + m_{H^+} - m_{NO_3^-} - m_{OH^-} = 0 \quad (26)$$

a sodium mass balance,

$$m^0_{NaOH} + m^0_{NaNO_2} - m_{Na^+} - m_{NaOH} - m_{(Na^+)(NO_3^-)} = 0 \quad (27)$$

a nitrogen mass balance,

$$m^0_{HNO_3} + m^0_{NaNO_2} - m_{HNO_3} - m_{NO_3^-} - m_{HNO_2} - m_{NO_2} - m_{NO} - 2m_{N_2O} - m_{(Na^+)(NO_3^-)} = 0 \quad (28)$$

and a redox balance,

$$m_{O_2} - \frac{1}{2}(m^0_{H_2O_2} - m^0_{NaNO_2} + m_{HNO_2}) - \frac{1}{4}(m_{NO_2} + 3m_{NO}) - 2m_{N_2O} = 0 \quad (29)$$

The equilibrium constants and extinction coefficients were fitted through a large-scale generalized reduced gradient (LSGRG2) optimization routine.[38] To properly scale the equations to aid optimization, a logarithmic transformation was made for each equation as described elsewhere.[72] The optimization was carried out on eight data sets corresponding to the different temperatures and pressures. Initially, all concentrations, extinction coefficients, and equilibrium constants were not bounded. These values were further refined by reducing the bounds of the variables to achieve more linear behavior in the log of the equilibrium constants versus density. Typically, the final values for the equilibrium constants were at least half an order of magnitude away from a bound.

Integrated areas of NO_2 and HNO_2 bands from deconvolution of the spectra were used in the determination of the equilibrium constants. The optimization was performed by using eqs 16−29 as constraints and the equilibrium constants, species concentrations, ionic strength, and activity coefficient as variables. Each of the eight data sets (T,P) included 35−48 experiments from classes I−IV (see Ziegler et al.[72]). This resulted in the simultaneous solution of 497−679 variables by using 490−672 equations as constraints. The objective function was chosen to be

$$\min\phi = w_1 \sum_{i=1}^{N} (A_{NO_2,\text{measured}} - \epsilon_{NO_2} l m_{NO_2})^2 + w_2 \sum_{i=1}^{N} (A_{HNO_2,\text{measured}} - \epsilon_{HNO_2} l m_{HNO_2})^2 \quad (30)$$

where ϵ_{NO_2}, and ϵ_{HNO_2} are the integrated extinction coefficients. The HNO_2 residuals were weighted so as to be the same order of magnitude as the NO_2 residuals; w_1 and w_2 were chosen to be 10 and 1000, respectively. This approach allowed the small integrated area of HNO_2 to affect the final equilibrium values. Further improvement to the model was achieved by applying the "jackknife" statistical procedure as described elsewhere.[72] Table 3 lists values of the equilibrium constants and molar absorptivities of NO_2 and HNO_2 obtained from the optimization. For a discussion of local optima and estimates on the error associated with these values see Ziegler et al.[72]

Figure 9 shows dissociation constants for nitric acid and the $(Na^+)(NO_3^-)$ ion pair plotted against the water density. Similarly to other strong acids, HNO_3 becomes a much weaker acid at high temperatures in supercritical water. Part of this effect is due to the exothermic character of HNO_3 dissociation at moderate and high densities. The second part is due to the isobaric decrease of water density and dielectric constant, which favor the associated species, i.e., HNO_3. The nitric acid dissociation constants at 380 °C agree well with the data of Marshall and Slusher obtained from calcium and magnesium sulfate solubilities in nitric acid solutions[25,26] at densities down to 0.45 g cm^{-3} (see Figure 9a). However, this new spectroscopic technique offers a means to measure equilibrium constants at very low densities, in this case down to 0.24 g cm^{-3}.

The dissociation constants for the $(Na^+)(NO_3^-)$ ion pair are close to corresponding data for NaCl, KCl, KOH, NaOH.[67,75,77] The change in $K_{d,ip}$ with a decrease in density (Figure 9b) reflects increased interionic interactions in low dielectric permittivity media.

Figures 10−13 show the equilibrium constants for reactions 4−7 plotted against the water density together with the gas-phase values calculated from existing thermodynamic data.[61] Reactions 4−7 are nonionic, and density effects on equilibrium constants are smaller than these observed for ionic reactions.[78] Linear extrapolation of the log K versus density plots to zero

TABLE 3: Equilibrium Constants for the Reactions 3−7 and 10 and Integrated Extinction Coefficients for NO_2 and HNO_2 from Optimization of the Measured NO_2 and HNO_2 Absorbances[a]

T °C	P MPa	$10^4\,K_{HNO_3}$ mol kg^{-1}	K_4 (mol kg^{-1})$^{0.5}$	$10^2\,K_5$	$10^2\,K_6$ (mol kg^{-1})$^{0.5}$	K_7 (mol kg^{-1})$^{0.5}$	$10^2\,K_{d,ip}$ mol kg^{-1}	$10^5\,\epsilon_{NO_2}$[b] (kg mol^{-1} cm^{-1}) cm^{-1}	$10^5\,\epsilon_{HNO_2}$[b] (kg mol^{-1} cm^{-1}) cm^{-1}
380	27.6	18.2	1.09	2.98	3.83	4.65×10^{-2}	4.65	6.24	1.43
	31.0	5.15	0.231	6.30	7.23	2.36×10^{-2}	12.3	6.40	1.77
	34.5	4.20	0.168	5.28	12.5	2.56×10^{-2}	5.13	6.05	2.39
	41.4	5.64	0.086	8.67	6.76	0.47×10^{-2}	16.6	6.04	2.16
400	27.6	0.006	24.4	0.05	41.6	490.91	0.003	7.06	7.46
	31.0	0.041	2.47	0.60	30.9	12.39	0.615	6.32	3.74
	34.5	0.586	1.06	2.17	22.8	0.53	0.582	6.68	2.08
	41.4	5.65	0.333	5.45	12.2	7.14×10^{-2}	5.15	7.08	1.82

[a] Class V experiments were not used in deconvolution. [b] Integrated extinction coefficient with respect to wavenumber (cm^{-1}).

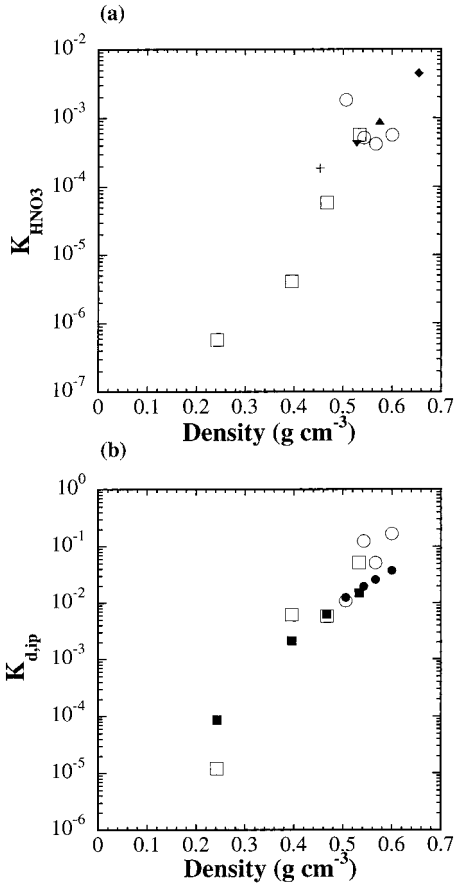

Figure 9. Dissociation constants of HNO_3 and the $(Na^+)(NO_3^-)$ ion pair at 380 °C (circles) and 400 °C (rectangles) plotted against solution density. (a) Literature data[25] for dissociation of saturated HNO_3 at 325 (◆), 350 (▲), 360 (▼), and 370 °C (+) are also presented. (b) For comparison, the literature data [77] for the dissociation of NaCl are also presented at identical temperatures and pressures (filled symbols).

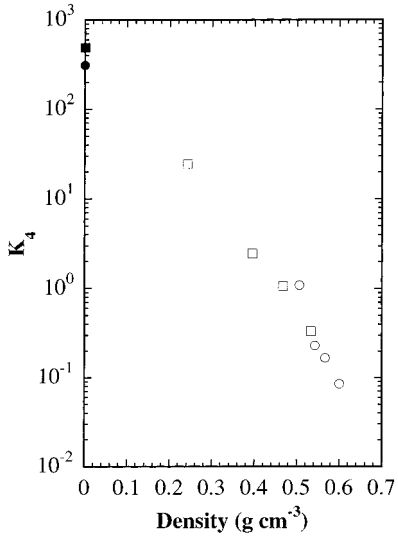

Figure 10. Equilibrium constants for reaction (4) in supercritical water at 380 °C (circles) and 400 °C (rectangles) plotted against solution density. For comparison, gas-phase data[61] calculated from thermochemical data are also presented (filled symbols).

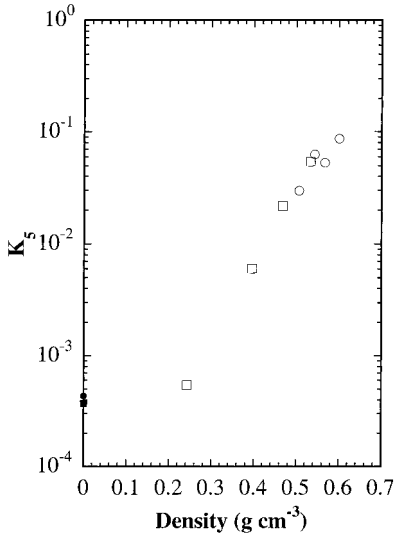

Figure 11. Equilibrium constants for reaction (5) in supercritical water at 380 °C (circles) and 400 °C (rectangles) plotted against solution density. For comparison, gas-phase data [61] calculated from thermochemical data are also presented (filled symbols).

density results in values which are very close to the gas-phase data, a result which supports our methodology. Relatively linear plots of log K vs ρ (in some cases log ρ) have been observed previously for equilibrium constants in hydrothermal solutions.[74]

The hydration of neutral molecules in SCW is most likely limited to the first coordination shell and is relatively weak.[39,79,80] For polar molecules such as HNO_3 and NO_2, the density effect is likely to be influenced more by the solvation energies resulting from dipole−dipole interactions than from partial molar volume changes.[81] The dipole moments for polar molecules in eqs 4−7 are 2.17 (HNO_3), 1.423 (*cis*-HNO_2), 1.855 (*trans*-HNO_2), 0.313 (NO_2), 0.159 (NO), 0.167 (N_2O), and 1.854 (H_2O).[82] A net decrease of dipole moment is observed for reactions 4, 6, and 7 on the basis of the stoichiometries. The observed decrease of the equilibrium constants with increasing density (dielectric constant) for these three reactions is consistent with this decrease in polarity. Similarly, the observed increase of the equilibrium constant for the disproportionation reaction 5 is consistent with the net increase in polarity upon the reaction.

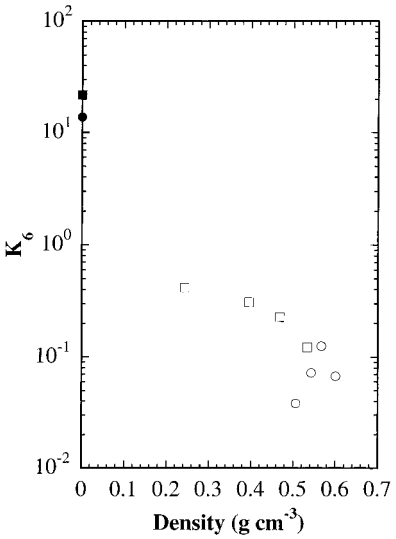

Figure 12. Equilibrium constants for reaction (6) in supercritical water at 380 °C (circles) and 400 °C (rectangles) plotted against solution density. For comparison, gas-phase data[61] calculated from thermochemical data are also presented (filled symbols).

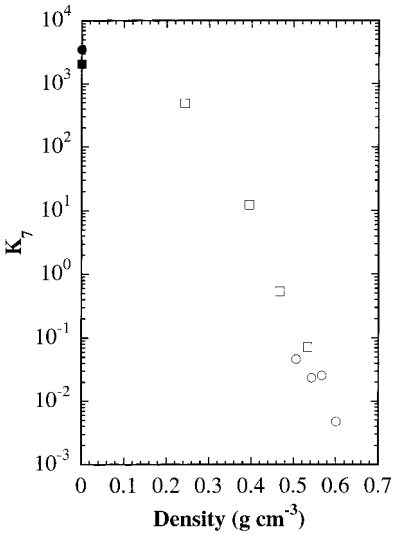

Figure 13. Equilibrium constants for reaction (7) in supercritical water at 380 °C (circles) and 400 °C (rectangles) plotted against solution density. For comparison, gas-phase data[61] calculated from thermochemical data are also presented (filled symbols).

Speciation Diagrams Based on the Regressed Equilibrium Constants. The concentrations of the various species in equilibrium were calculated from eqs 16−29 on the basis of the feed concentrations and equilibrium constants regressed from the model. The results obtained at 380 °C and 31 MPa for three classes (I, III, and IV) are presented in Figures 14−16, respectively. For pure nitric acid solutions (class I, Figure 14), the concentration of each species increases in approximately the same manner with an increase in the feed HNO_3 concentration. This result is consistent with the relatively constant HNO_2 to NO_2 molar ratio in Figure 4.

The addition of H_2O_2 reduces the decomposition of HNO_3 modestly (Figure 15). The relative decrease in the concentrations of the products follows the order N_2O (from 10^{-6} to 10^{-10} mol kg^{-1}, not shown) > NO > HNO_2 > NO_2, a result consistent with the oxidation states of nitrogen. The weak decrease in NO_2 concentration shown in Figure 15 was not observed experimentally over the whole range of H_2O_2 concentrations. A decrease followed by a small increase of the NO_2 content was actually

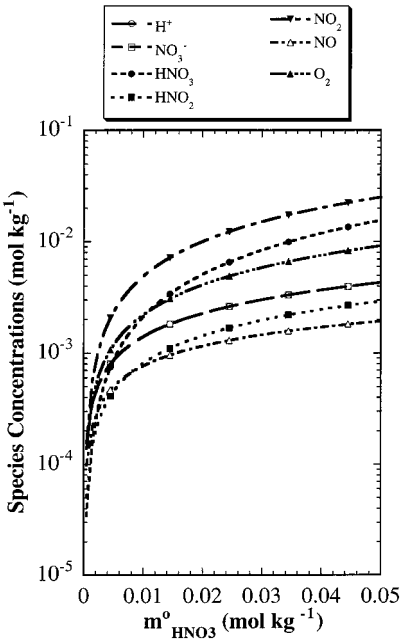

Figure 14. Speciation diagram of the major species in class I experiments at 380 °C and 31.0 MPa.

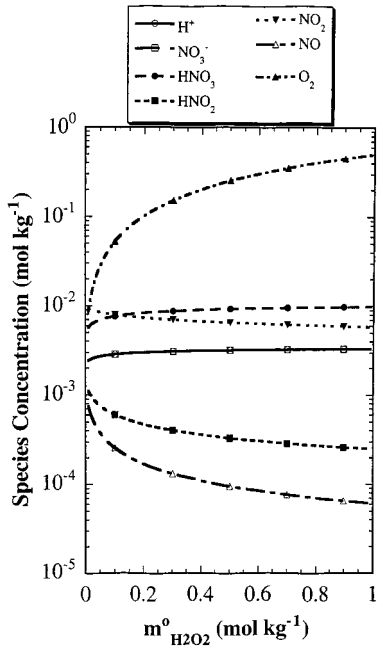

Figure 15. Speciation diagram of the major species in class III experiments at 380 °C and 31.0 MPa. The initial concentration of HNO_3 is 0.0232 mol kg^{-1}.

observed at 380 °C (Figure 5) but not at 400 °C. This behavior may result in part from the error introduced in correcting the measured absorbances (Figure 5) for density when the actual solution density is approximated by the water density at the same *T* and *P*. Electrolytes increase the density, and the actual concentration of ions increases upon addition of H_2O_2 (Figure 15). Therefore, the density corrected absorbances will be progressively overestimated as the H_2O_2 feed concentration increases.

Addition of $NaNO_2$ to a HNO_3 solution (Figure 16) leads to a significant increase in the N_2O and NO concentrations and to a substantial decrease in oxygen concentration. These changes may be understood easily. Addition of an N (+3) species ($NaNO_2$) to a solution of N (+5) species (HNO_3) destabilizes

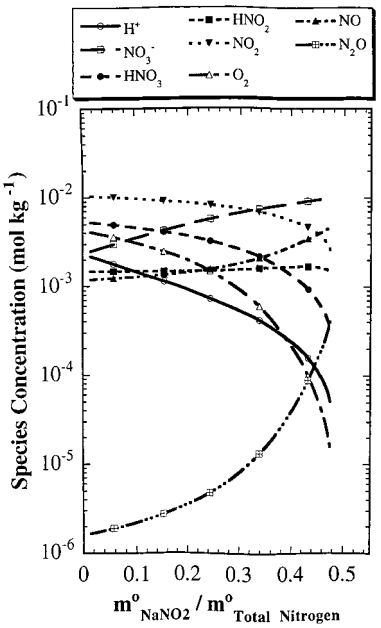

Figure 16. Speciation diagram of the major species in class IV experiments at 380 °C and 31.0 MPa. Total nitrogen concentration is 0.0208 mol kg^{-1}.

products with an oxidation state higher than +3 (NO_2, sum of nitrate ion and nitric acid) and stabilizes products with an oxidation state lower than +3 (N_2O, NO). A relatively constant concentration is observed for HNO_2. The small increase in NO_3^- concentration upon addition of $NaNO_2$ is caused by an increase in OH^- concentration (from 10^{-10} to 10^{-8} mol kg^{-1}, not shown) resulting from the decrease in the HNO_3 feed concentration and increase in $NaNO_2$, which exhibits basic properties.

The quantitative predictions of our model (see above, Figures 14−16) agree very well with the measured HNO_2 and NO_2 absorbance bands. Examples include the roughly proportional increase of both HNO_2 and NO_2 bands generated by an increase in HNO_3 concentration (Figures 4 and 14), the relative effect of oxygen on the NO_2 and HNO_2 bands (Figures 5 and 15), and the weak sensitivity of the HNO_2 band in the $HNO_3/NaNO_2$ mixtures to the solution composition (Figures 7 and 16).

The predictions of the model for the species whose absorbances were not measured directly also appear to be realistic. Class IV (mixtures of HNO_3 and $NaNO_2$) experiments (Figure 7) suggested that significant amounts of a species with a nitrogen oxidation state lower than +3 were formed. Indeed, a significant contribution from NO is predicted by the model (Figure 16). Concentration changes for other species including HNO_3, NO_3^-, N_2O, oxygen, and the ion pairs NaOH and $(Na^+)(NO_3^-)$ follow trends, which may be expected from the feed solution composition and/or oxidation state of nitrogen.

Conclusions

Chemical equilibria in nitric acid solutions in SCW may be measured directly from the absorbance bands of NO_2 and HNO_2 from 380−400 °C by UV−vis spectroscopy. These absorbance bands are similar to those at ambient temperature, except the fine structure of NO_2 is far less than that in the gas phase. All of the spectra appear to be nearly completely reversible upon cooling. Equilibrium constants for reactions 3−7 and 10 can be determined by optimization of the measured and calculated absorbances of NO_2 and HNO_2. Other important decomposition products that do not absorb in the wavelengths studied include O_2, NO, and, in mixtures of HNO_3 and $NaNO_2$, N_2O.

The equilibrium constants for all the reactions change with water density in the direction expected, on the basis of the change in polarity. In most cases, the measured equilibrium constants are in good agreement with the gas-phase value when extrapolated to zero density. While the behavior of ionic reactions 3 and 10 may be quantified in terms of a modified Born model,[33,36] nonionic reactions 4−7 require other types of models to predict solvation effects.[79] These models are useful for extrapolation of the equilibrium constants to even higher temperatures, which are also of interest in hydrothermal technology.

Acknowledgment. We gratefully acknowledge support from the Department of Energy (DE-FG07-96ER14687), from the U.S. Army for a University Research Initiative Grant (30374-CH-URI), from the R.A. Welch Foundation, and from the Separations Research Program at the University of Texas, a consortium of over 30 companies.

References and Notes

(1) Miller, J. A.; Bowman, C. T. *Prog. Energy Combust. Sci.* **1989**, *15*, 287.
(2) Wendel, M. M.; Pigford, R. L. *AIChE J.* **1958**, *4*, 249.
(3) England, C.; Corcoran, W. H. *Ind. Eng. Chem. Fundam.* **1974**, *13*, 373.
(4) Kaiser, E. W.; Wu, C. H. *J. Phys. Chem.* **1977**, *81*, 187.
(5) Kaiser, E. W.; Wu, C. H. *J. Phys. Chem.* **1977**, *81*, 1701.
(6) Odenbrand, C. U. I.; Andersson, L. A. H.; Brandin, J. G. M.; Lundin, S. T. *Appl. Catal.* **1986**, *27*, 363.
(7) Kiovsky, J. R.; Koradia, P. B.; Lim, C. T. *Ind. Eng. Chem. Prod. Res. Dev.* **1980**, *19*, 218.
(8) Kato, A.; Matsuda, S.; Kamo, T.; Nakajima, F.; Kuroda, H.; Narita, T. *J. Phys. Chem.* **1981**, *85*, 4099.
(9) Tester, J. W.; Holgate, H. R.; Armellini, F. J.; Webley, P. A.; Killilea, W. R.; Hong, G. T.; Barner, H. E. In *Emerging Technologies in Hazardous Waste Management*; Tedder, D. W., Pohland, F. G., Ed.; ACS Symposium Series 518; American Chemical Society: Washington, DC, 1993; pp 35−76.
(10) Gloyna, E. F.; Li, L. *Waste Manage.* **1993**, *13*, 379.
(11) Killilea, W. R.; Swallow, K. C.; Hong, G. T. In *2nd International Symposium on Supercritical Fluids*; Department of Chemical Engineering, Johns Hopkins University: Boston, MA, 1991; pp 173−176.
(12) Dell'Orco, P. C. Ph.D. Dissertation Thesis, University of Texas at Austin, 1994.
(13) Dell'Orco, P. C.; Foy, B. F.; Robinson, J. M.; Buelow, S. J. *Haz. Waste Haz. Mater.* **1993**, *10*, 221.
(14) Dell'Orco, P.; Foy, B.; Wilmanns, E.; Le, L.; Ely, J.; Patterson, K.; Buelow, S. In *Innovations in Supercritical Fluids. Science and Technology*; Hutchenson, K. W., Foster, N. R., Ed.; American Chemical Society: Washington, D. C., 1995; pp 179−196.
(15) Oldenborg, R.; Robinson, J. M.; Buelow, S. J.; Dyer, R. B.; Anderson, G.; Dell'Orco, P. C.; Funk, K.; Willmanns, E.; Knutsen, K. *Hydrothermal Processing of Inorganic Components of Hanford Tank Wastes*; Los Alamos National Laboratories report LA-UR-94:3233; Los Alamos National Laboratories, 1994.
(16) Proesmans, P. I.; Luan, L.; Buelow, S. J. *Ind. Eng. Chem. Res.* **1997**, *36*, 1559.
(17) Adschiri, T.; Kanazawa, K.; Arai, K. *J. Am. Ceram. Soc.* **1992**, *75*, 2615.
(18) Adschiri, T.; Kanazawa, K.; Arai, K. *J. Am. Ceram. Soc.* **1992**, *75*, 1019.
(19) Shoppelrei, J. W.; Brill, T. B. *J. Phys. Chem. A* **1997**, *101*, 8593.
(20) Shoppelrei, J. W.; Kieke, M. L.; Wang, X.; Klein, M. T.; Brill, T. B. *J. Phys. Chem.* **1996**, *100*, 14343.
(21) Maiella, P. G.; Brill, T. B. *Appl. Spectrosc.* **1996**, *50*, 829.
(22) Spohn, P. D.; Brill, T. B. *J. Phys. Chem.* **1989**, *93*, 6224.
(23) Ratcliffe, C. I.; Irish, D. E. *Can. J. Chem.* **1985**, *63*, 3521.
(24) Oscarson, J. L.; Gillespie, S. E.; Izatt, R. M.; Chen, X.; Pando, C. *J. Solution Chem.* **1992**, *21*, 789−801.
(25) Marshall, W. L.; Slusher, R. *J. Inorg. Nucl. Chem.* **1975**, *37*, 2165.
(26) Marshall, W. L.; Slusher, R. *J. Inorg. Nucl. Chem.* **1975**, *37*, 1191.
(27) Marshall, W. L.; Jones, E. V. *J. Inorg. Nucl. Chem.* **1974**, *36*, 2313.
(28) Barton, C. J.; Hebert, G. M.; Marshall, W. L. *J. Inorg. Nucl. Chem.* **1961**, *21*, 141.
(29) Seward, T. M. *Geochim. Cosmochim. Acta* **1984**, *48*, 121.
(30) Heinrich, C. A.; Seward, T. M. *Geochim. Cosmochim. Acta* **1990**, *54*, 2207.

(31) Gammons, C. H.; Seward, T. M. *Geochim. Cosmochim. Acta* **1996**, *60*, 4295.
(32) Chlistunoff, J. B.; Johnston, K. P. *J. Phys. Chem. B* **1998**, *102*, 3993.
(33) Xiang, T.; Johnston, K. P. *J. Phys. Chem.* **1994**, *98*, 7915.
(34) Xiang, T.; Johnston, K. P.; Wofford, W. T.; Gloyna, E. F. *Ind. Eng. Chem. Res.* **1996**, *35*, 4788.
(35) Xiang, T.; Johnston, K. P. *J. Solution Chem.* **1997**, *26*, 13.
(36) Ryan, E. T.; Xiang, T.; Johnston, K. P.; Fox, M. A. *J. Phys. Chem. A* **1997**, *101*, 1827.
(37) Shin, T. W.; Kim, K.; Lee, I.-J. *J. Solution Chem.* **1997**, *26*, 379.
(38) Smith, S.; Lasdon, L. *J. Comput.* **1992**, *4*, 1.
(39) Bennett, G. E.; Johnston, K. P. *J. Phys. Chem.* **1994**, *98*, 441.
(40) *Official Methods of Analysis of AOAC International*, 16th ed.; AOAC International: Arlington, 1995; Vol. II, pp A.1.12.
(41) Kolthoff, I. M.; Sandell, E. B. *Textbook of Quantitative Inorganic Analysis*, 3rd ed.; The Macmillan Company: New York, 1952.
(42) Hall, T. C.; Blacet, F. E. *J. Chem. Phys.* **1952**, *20*, 1745.
(43) Norris, M. S.; Fleck, S. A.; Lichtenfels, D. H. *Anal. Chem.* **1955**, *27*, 1565.
(44) Schneider, W.; Moortgat, G. K.; Tyndall, G. S.; Burrows, J. P. *J. Photochem. Photobiol.* **1987**, *40*, 195.
(45) Mihalcea, R. M.; Baer, D. S.; Hanson, R. K. *Appl. Optics* **1996**, *35*, 4059.
(46) Chao, J.; Wilhott, R. C.; Zwolinski, B. J. *Thermochim. Acta* **1974**, *10*, 359.
(47) Hisatsune, I. C. *J. Phys. Chem.* **1961**, *65*, 2249.
(48) McLane, C. K. *J. Chem. Phys.* **1949**, *17*, 379.
(49) Takagi, J.; Ishigure, K. *Nucl. Sci. Eng.* **1985**, *89*, 177.
(50) Strickler, S. J.; Kasha, M. *J. Am. Chem. Soc.* **1963**, *85*, 2899.
(51) Longstaff, J. V. L.; Singer, K. *J. Chem. Soc.* **1954**, 2604.
(52) Bunton, C. A.; Stedman, G. *J. Chem. Soc.* **1958**, 2440.
(53) Bayliss, N. S.; Watts, D. W. *Aust. J. Chem.* **1956**, *9*, 319.
(54) Bennet, M. R.; Brown, G. M.; Maya, L.; Posey, F. A. *Inorg. Chem.* **1982**, *21*, 2461.
(55) Wikstrom, M. M.; Nobe, K. *I&EC Process Des. Dev.* **1965**, *4*, 191.
(56) Sponer, H.; Bonner, L. G. *J. Chem. Phys.* **1940**, *8*, 33.
(57) Friend, J. A.; Lyons, L. E. *J. Chem. Soc.* **1959**, 1572.
(58) Mason (Banus), J. *J. Chem. Soc.* **1959**, 1288.
(59) Beattie, I. R.; Vosper, A. J. *J. Chem. Soc.* **1961**, 2106.
(60) Verhoek, F. H.; Daniels, F. *J. Am. Chem. Soc.* **1931**, *53*, 1250.
(61) Chase, M. W., Jr.; Davies, C. A.; Downey, J. R., Jr.; Frurip, D. J.; McDonald, R. A.; Syverud, A. N. *JANAF Thermochemical Tables*, 3rd ed.; American Chemical Society and the American Institute of Physics for the National Bureau of Standards, 1985; Vol. 14.
(62) Lumme, P.; Lahermo, P.; Tummavuori, J. *Acta Chem. Scand.* **1965**, *19*, 2175.
(63) Lumme, P.; Tummavuori, J. *Acta Chem. Scand.* **1965**, *19*, 617.
(64) Tummavuori, J.; Lumme, P. *Acta Chem. Scand.* **1968**, *22*, 2003.
(65) Mesmer, R. E.; Marshall, W. L.; Palmer, D. A.; Simonson, J. M.; Holmes, H. F. *J. Solution Chem.* **1988**, *17*, 699.
(66) Chen, X.; Izatt, R. M.; Oscarson, J. L. *Chem. Rev.* **1994**, *94*, 467.
(67) Ho, P. C.; Palmer, D. A. *Geochim. Cosmochim. Acta* **1997**, *61*, 3027.
(68) Dixon, J. K. *J. Chem. Phys.* **1940**, *8*, 157.
(69) Nakayama, T.; Kitamura, M. Y.; Watanabe, K. *J. Chem. Phys.* **1959**, *30*, 1180.
(70) Corcoran, T. C.; Beiting, E. J.; Mitchell, M. O. *J. Mol. Spectrosc.* **1992**, *154*, 119.
(71) Armerding, W.; Walter, J.; Ruger, Chr.; Spiekermann, M.; Comes, F. J. *Ber. Bunsen-Ges. Phys. Chem.* **1993**, *97*, 1440.
(72) Ziegler, K. J.; Chlistunoff, J.; Lasdon, L.; Johnston, K. P., 1999, submitted.
(73) Singer, K.; Vamplew, P. A. *J. Chem. Soc.* **1956**, 3971.
(74) Marshall, W. L.; Franck, E. U. *J. Phys. Chem. Ref. Data* **1981**, *10*, 1.
(75) Ho, P. C.; Palmer, D. A. *J. Solution Chem.* **1996**, *25*, 711.
(76) Pitzer, K. S. In *Activity Coefficients in Electrolyte Solutions*, 2nd ed.; CRC Press: Boca Raton, 1991; pp 75−153.
(77) Ho, P. C.; Palmer, D. A.; Mesmer R. E. *J. Solution Chem.* **1994**, *23*, 997.
(78) Balbuena, P. B.; Johnston, K. P.; Rossky, P. J. *J. Phys. Chem.* **1996**, *100*, 2706.
(79) Luo, H.; Tucker, S. C. *J. Phys. Chem.* **1997**, *101*, 1063.
(80) Sitkoff, D.; Sharp, K. A.; Honig, B. *J. Phys. Chem.* **1994**, *98*, 1978.
(81) Ji, Q. E. M. E.; van Eldik, R.; Johnston, K. P.; Goates, S. R.; Lee, M. L. *J. Phys. Chem.* **1995**, *99*, 13461.
(82) *CRC Handbook of Chemistry and Physics*, 78th ed.; CRC Press: Boca Raton, 1997.